

# Self-Lubricative Organic-Inorganic Hybrid Coating with Anti-Icing and Anti-Waxing Performances by Grafting Liquid-Like Polydimethylsiloxane

Xiaoqing Hao, Zhengrong Sun, Shuwang Wu, Ta-Wei Wang, Yubo Liu, Yang Wu,\* Ximin He, Qinze Liu,\* and Feng Zhou

Polydimethylsiloxane (PDMS) is one of the most popular materials to protect infrastructures from the complicated environment due to its chemical stability, nontoxicity, low cost, high durability, and chain flexibility. Herein, a series of organic-inorganic hybrid coatings are prepared by simply grafting loop-like PDMS on a solid surface. Owning to the low surface energy and high mobility of PDMS chains, the special characteristics, including liquid repellency, anti-fouling, self-lubrication, anti- and delay-ice, anti-paraffin, etc., are presented. To confirm the liquid-like slippery nature of PDMS surface, the controlled de-icing and de-waxing tests on rigid chain surfaces are conducted. The liquid-like nature of PDMS allows ice or paraffin to have a low adhesion in a slip state, but a fractured state on alkylated and perfluorinated surface with a high adhesion strength. In addition, the flexible PDMS chains grafted on the inorganic silica layer by stable covalent bond endow the surface with excellent durability, including maintaining low ice adhesion during 50 icingdeicing cycles, resistance to UV irradiation, washing or soaking in organic solvent, etc. This work provides a simple approach for constructing self-lubricative low surface energy coating to realize de-ice and de-wax easily, which may have a broad prospect of application in equipment protection.

X. Hao, Q. Liu

School of Materials Science and Engineering

Qilu University of Technology (Shandong Academy of Sciences)

Jinan, Shandong 250353, P. R. China

E-mail: liuqinze@qlu.edu.cn

X. Hao, Z. Sun, Y. Liu, Y. Wu, F. Zhou

State Key Laboratory of Solid Lubrication

Lanzhou Institute of Chemical Physics Chinese Academy of Science

Lanzhou, Gansu 730000, P. R. China

E-mail: yangwu@licp.cas.cn

Z. Sun, Y. Liu, Y. Wu

Qingdao Centre of Resource Chemistry and New Materials

Qingdao, Shandong 266100, P. R. China

S. Wu, T.-W. Wang, X. He

Department of Material Science and Engineering

University of California

Los Angeles, CA 90095, USA

Y. Wu

Yantai Zhongke Research Institute of Advanced Materials and Green Chemical Engineering

Shandong Laboratory of Advanced Materials and Green Manufacturing Yantai, Shandong 264006, P. R. China



The ORCID identification number(s) for the author(s) of this article can be found under https://doi.org/10.1002/admi.202200160.

DOI: 10.1002/admi.202200160

#### 1. Introduction

In the past two decades, low surface energy coatings have been widely reported because of special surface wettability that plays a vital role in addressing issues ranging from daily life to industrial and agricultural production.<sup>[1]</sup> Inspired by the lotus leaf, [2] superhydrophobic surface with a contact angle (CA) larger than 150° and sliding angle (SA) lower than 10° has been developed and widely applied in self-cleaning, antifouling, anti-icing/ frosting,[3a,5] anticorrosion.<sup>[6]</sup> paraffin,[7] drag reduction,[8] and oil/water mixture separation,<sup>[9]</sup> etc. The principle of fabricating superhydrophobic surface was based on the combination of micro/ nano-scale hierarchical structures and low surface energy chemical modification. [3b,10] The hierarchical texture was conducive to the formation of retained air pockets that minimized solid-liquid contact area and repelled water droplets adhesion via

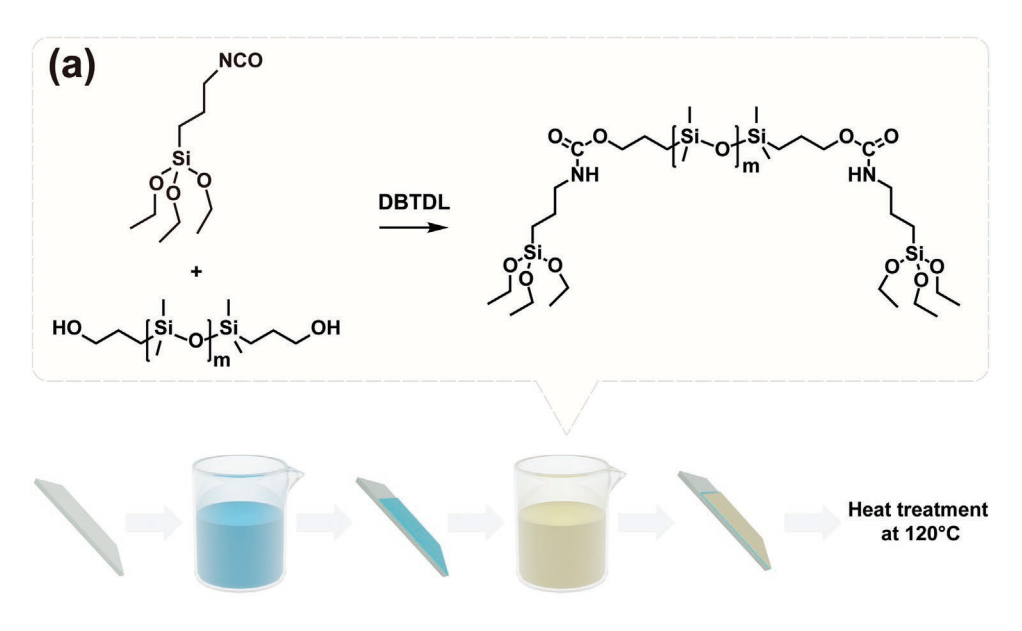
a non-wetting Cassie state.[11] However, the superhydrophobic surface was brittle and destroyed easily even under a small mechanical load friction.[3b,12] In addition, the non-wetting superhydrophobic state was metastable, and the trapped air could be replaced by vapor or micro-contaminants, which resulted in the surface wettability transition from Cassie-Baxter state to Wenzel state. [13] To avoid the unstable air pockets, slippery liquid-infused porous surfaces (SLIPS) enlightened from Nepenthes pitcher plants emerged.[14] To make SLIPS, a low surface energy lubricate liquid was infused into a rough micro/ nanoporous substrate to construct continuous and homogeneous versatile surfaces. The SLIPS showed extreme slipperiness and low contact angle hysteresis of various liquids, thus preventing stable attachment of fouling organisms and easily repelling various immiscible liquid pollutants, including low surface tension liquids, blood, and crude oil.[15] Moreover, the outstanding anti-icing (long-delayed icing time ≈100 min)[16] and de-icing (ultralow ice adhesion, less than 20 kPa)[17] performances were found on the SLIPS because of the existence of mobile liquid film.  $^{[18]}$  However, there are obvious drawbacks of SLIPS based on the design principle. For example, the lubricant molecules attached to the surface by weak Van der Waals force were easy to lose after repeated contact testing and the brittle

micro-nano structures of SLIPS cannot endure mechanical wear, etc.  $^{[19]}$ 

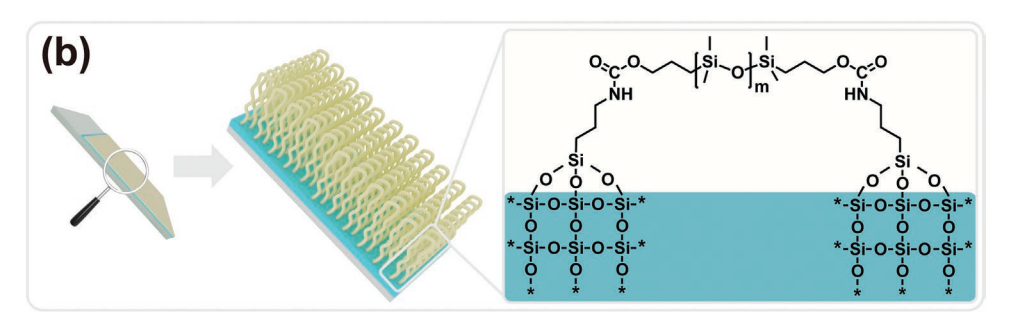
To improve the limitations of texture and lubricants and to achieve a more ideal and durable SLIPS material, the liquid-like surfaces by covalently grafting flexible molecular chains to a smooth surface have been developed. [20] Polydimethylsiloxane (PDMS), the traditional lubricant molecule, was widely used to construct the liquid-like surface due to its mobility, chemical stability, nontoxicity, hydrophobicity, and relatively high durability. [20g,21] By in situ acid-catalyzed polycondensation of dimethyldimethoxysilane, the liquidlike PDMS brushes were grafted on the smooth hydroxylated surface to give the surface slippery omniphobicity.<sup>[20c]</sup> By the terminal group instant reaction, the PDMS brushes were also grafted to a solid surface to render slippery omniphobicity.[22] Liu's group successfully developed a series of transparent anti-smudge coatings by adding PDMS into commercial polyurethane and epoxy resin, which are suitable for various substrates and can maintain liquid repellency for a long time. [20f,h,23] Wang et al [24] fabricated a liquid-entrenched smooth surface that can reduce the adhesion of viscoelastic solids compared to the superhydrophobic surface and

traditional SLIPS materials, which has a wide application in bathroom facilities. Recently, the outstanding de-icing property of covalent tethered PDMS coatings also was involved, and the interesting interface slip caused by the flexibility and liquid-like property of PDMS surface was revealed. [20b,d,g]

In this work, we have prepared a series of low surface energy organic-inorganic hybrid PDMS coatings with liquid-repellent, antifouling, self-lubricating, anti- & delay-ice, and anti-wax properties by simple dip-coating technology. Functionalized terminal groups of PDMS were grafted onto the inorganic silica sol layer to ensure stability and durability, and the unbound movable parts of the chain given the surface self-lubricative and liquid-like properties. In addition, the heterogeneous nucleation ice was suppressed, and distinct antifrosting was shown on the hybrid PDMS coating. In de-icing and de-waxing tests, the organic-inorganic hybrid PDMS surface allows ice or wax to separate with the slippery state under low shear force, yet showed high shear force on alkylated and perfluorinated surfaces with the fractured state. This work provides a simple approach to construct self-lubricative low surface energy coating to realize de-ice and de-wax easily, which may have a broad prospect of application in equipment protection.



Dipping in silica sol Dipping in loop-polydimethylsiloxane



Scheme 1. Schematic illustration of a) the preparation process of the glass@silica sol@loop-like PDMS and b) the chemical structures of the glass@silica sol@loop-like PDMS.

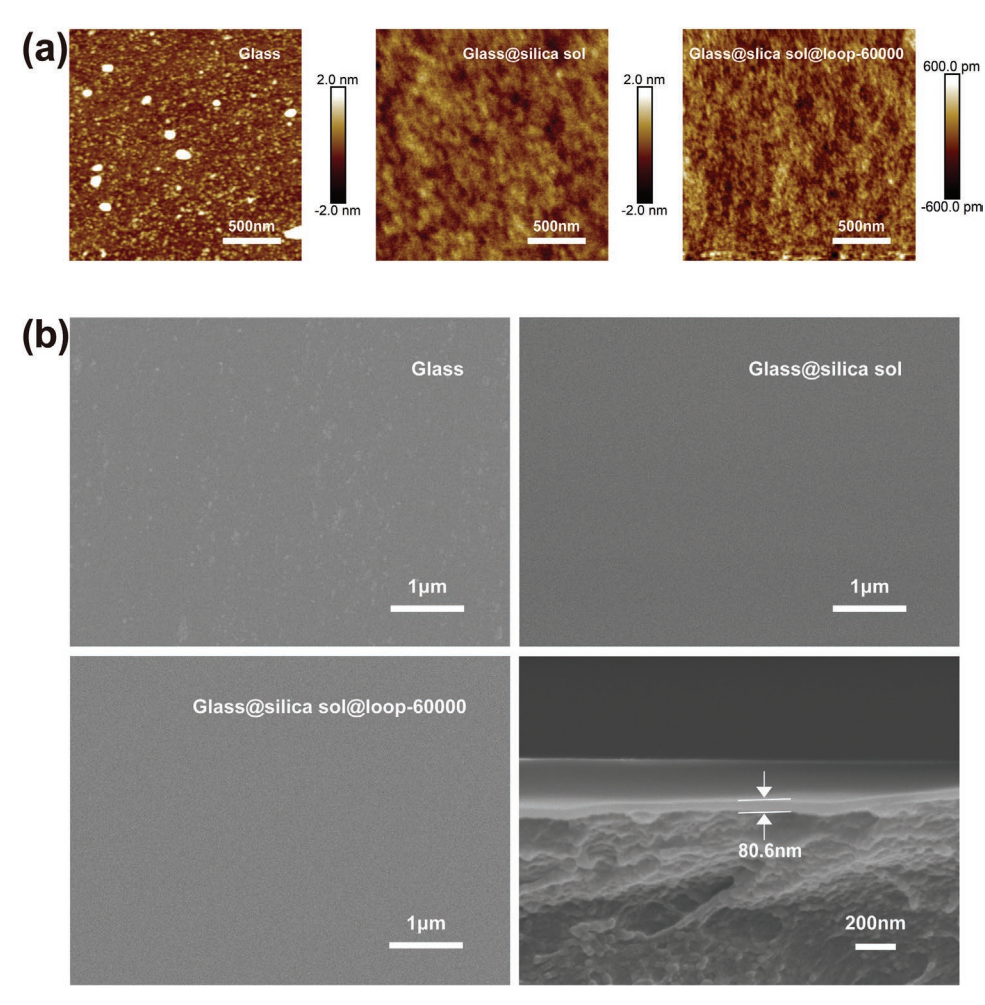


Figure 1. a) AFM and b) SEM images of glass, glass@silica sol and glass@silica sol@loop-60000, and the SEM image of the cross profile of hybrid coating.

#### 2. Results and Discussion

#### 2.1. Preparation of Loop-Like PDMS Polymer

The preparation process of loop-like PDMS polymer and organic-inorganic hybrid coating is shown in Scheme 1a. To fabricate the self-lubricative organic-inorganic hybrid coating, firstly, a layer of inorganic silica sol was deposited on a clean glass sheet to establish an inorganic layer, then the loop-like PDMS chains were decorated on the inorganic silica sol layer by a simple dipping coating procedure. At last, the substrate was heated to 120 °C for 30 min to hard the hybrid coating. During the heating process, the hydrolysates of triethoxysilane of the loop-like PDMS and the silicon hydroxyl groups on the inorganic silica sol layer were dehydrated to form a stable Si-O-Si bond, and the loop-like PDMS chains were grafted to the silica sol layer with both ends (Scheme 1b). Figure 1a exhibits the atomic force microscopy (AFM) images of specimens at different preparation stages, and the roughness of different specimen surfaces was summarized in Table S1 (Supporting Information). As shown in Figure 1a, there were many random nano-defects on the raw glass surface and a large roughness was presented (Rq = 0.562 nm). After depositing a layer of silica sol, the nano-defects disappeared, and the roughness was reduced to 0.331 nm, which means that the nano-defects on raw glass surface were filled up and made the surface flatter. After grafting loop-60000, the glass@silica sol@loop-60000 surface became extraordinarily flat, and the roughness was reduced to 0.118 nm, which presented a totally different morphology on glass@loop-60000 surface without silica sol layer. On the surface of glass@loop-60000, there were countless bright nanodots of different sizes (Figure S1a, Supporting Information) that could be attributed to the aggregation of loop-60000 polymers. On silica sol surface, sufficiently active sites (Si-OH) were provided to bond with the loop-60000 PDMS and showed a better affinity than the raw glass surface which may lead to the flat surface morphology. The scanning electron microscopy (SEM) images of coating surfaces also confirmed the same results, as shown in Figure 1b. The raw glass had obvious protrusions, while the glass surface modified by the silica sol became flat. There were many nano-protrusions unevenly dispersed on the surface of glass@loop-like PDMS (Figure S1, Supporting Information), while without any nano-protrusions on glass@silica sol@loop-like PDMS surface. From the cross-section SEM image of the hybrid coating, the thickness of this coating was ≈80.6 nm.

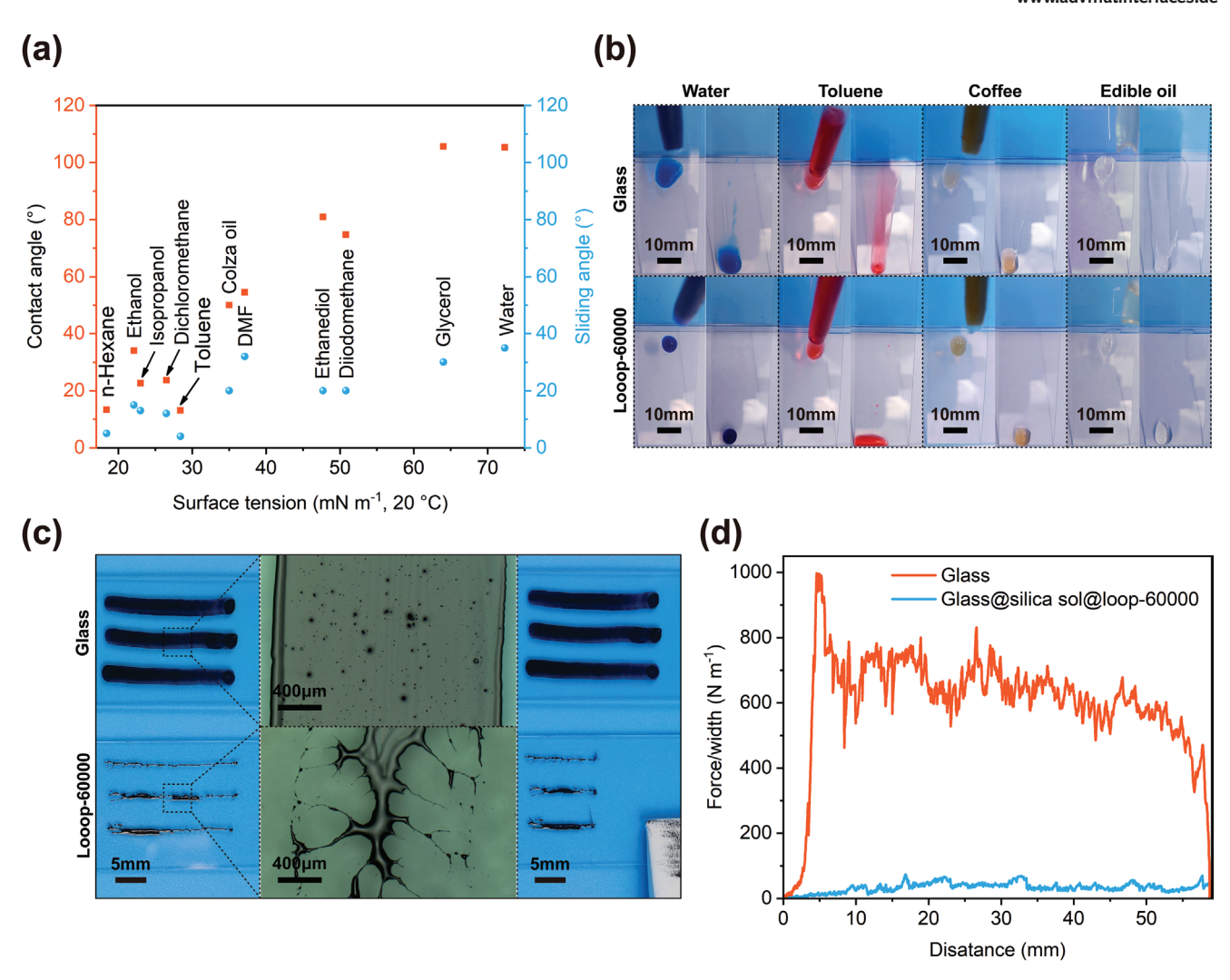


Figure 2. a) The variation of CAs and SAs of liquid droplets ( $20 \,\mu\text{L}$ ) with surface tensions on glass@silica sol@loop-60000 surface. b) The comparison of self-cleaning property of water, toluene, coffee, edible oil on glass and glass@silica sol@loop-60000 surfaces. c) Ink-resistant test by an oil-based permanent marker on glass and glass@silica sol@loop-60000 surfaces. d) The peel strength of 3 M tape on glass and glass@silica sol@loop-60000 surfaces.

# 2.2. Liquid Repellency and Stain Resistance of the Hybrid Coating Surface

After decorating the hybrid coating, the glass surface became hydrophobic, and the water CA on glass@silica sol@loop-60000 reached 106° (Figure S2, Supporting Information). The CAs and SAs of various liquids with different surface tensions on the glass@silica sol@loop-60000 surface were also discussed. As can be seen in Figure 2a, with the surface tension increased from 18.43 mN  $m^{-1}$  (n-hexane) to 72.8 mN  $m^{-1}$  (water), the CA of liquid droplets gradually improved from 11° to 106°. Crucially, all the droplets could slide off from the glass@silica sol@loop-60000 surfaces even with a small CA, which indicated a low adhesion drag on glass@silica sol@loop-60000 for these liquid droplets. The surface energy of glass@silica sol@loop-60000 coating was calculated to be about 25.48 mJ  $\,\mathrm{m}^{-2}$  by the Owens method.<sup>[25]</sup> Benefited from the excellent liquid repellency, the glass@silica sol@loop-60000 has excellent self-cleaning and anti-fouling property, as is exhibited in Figure 2b and Movie S1

(Supporting Information). A water droplet dyed with methylene blue slid across the raw glass surface and left water traces, but the water droplet floated away from the glass@silica sol@ loop-60000 surface without leaving any traces. Similar situations were presented for toluene, coffee, edible oil, etc. The ink-resistant test was carried out to further prove its exceptional stain resistance performance. As shown in Figure 2c, an oil-based permanent marker could write on the raw glass surface easily and a continuous and uniform ink trace could be observed under the optical microscope, while it was difficult to write on the glass@silica sol@loop-60000 surface and a disconnected and uneven ink track was observed. Interestingly, the uneven ink track on glass@silica sol@loop-60000 surface was easy to wipe away with tissue paper, yet there was no noticeable change on the raw glass surface after wiping with tissue paper. The glass@silica sol@loop-60000 also displayed distinguished anti-affixing properties (Figure 2d), the average peeling strength of 3 M adhesive tape on the glass@silica sol@loop-60000 surface was 33.85 N m<sup>-1</sup> which was only about one-eighteenth of

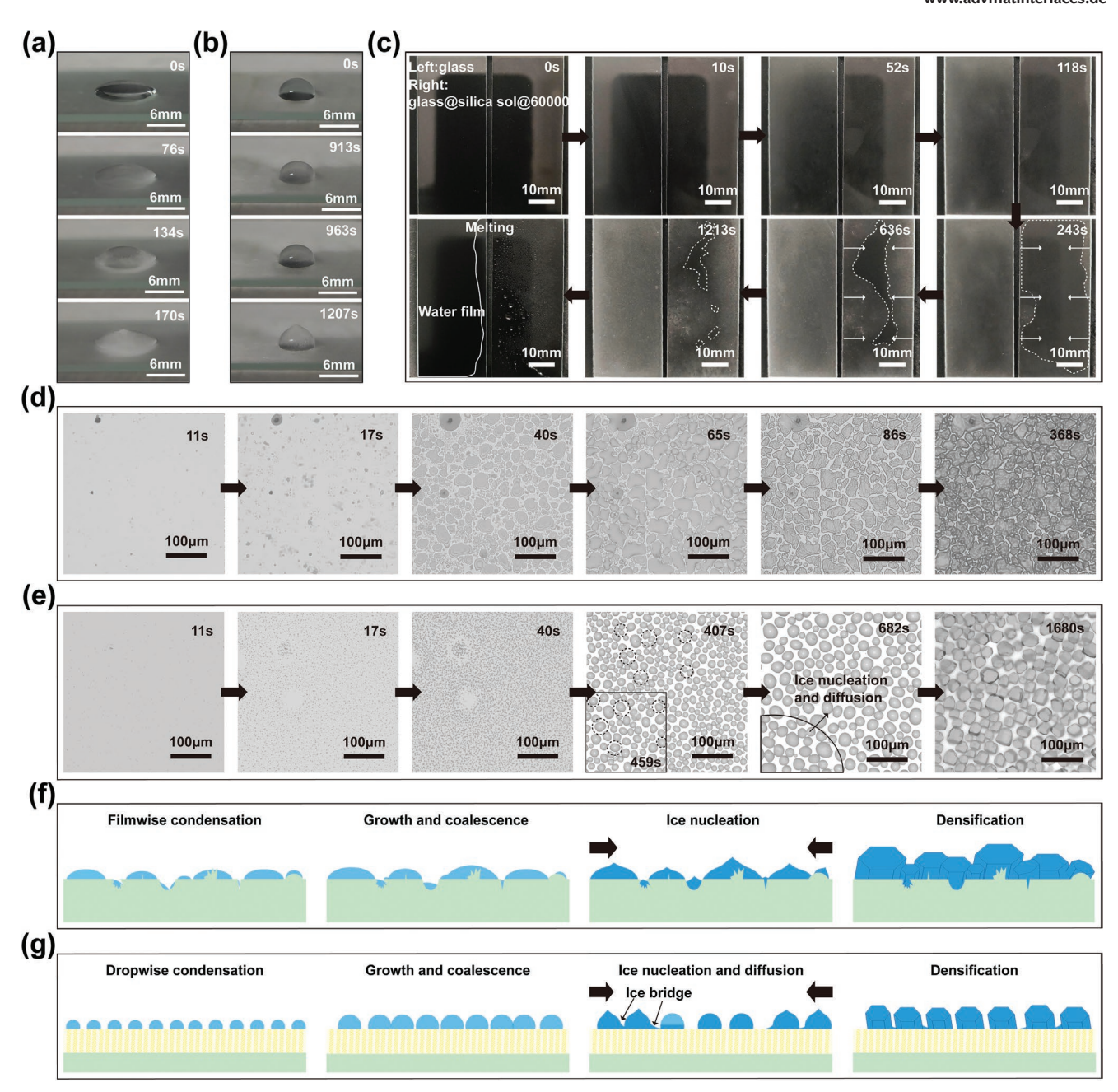


Figure 3. Photographs of a water droplet freeze on a) glass and b) glass@silica sol@loop-60000 surfaces during the whole icing process. c) Photographs of the macroscopical frost-formation on glass and glass@silica sol@loop-60000 surfaces during the whole frosting and frost melting process (In the photograph at the same moment, the glass surface was on the left and the glass@silica sol@loop-60000 was on the right). Time-lapse images of the microscopic frost-formation on d) glass and e) glass@silica sol@loop-60000 surfaces. Schematic of the entire condensation and frosting process on f) glass and g) glass@silica sol@loop-60000 surfaces.

the average peeling strength of 3 M adhesive tape on raw glass surface (598.65 N  $\rm m^{-1}).$ 

# 2.3. Delay Icing and Delay Frosting on the Hybrid Coating Surface

The anti-icing property of glass@silica sol@loop-60000 surface was assessed by icing delay time of a water droplet. Icing

delay time of a water droplet on glass and glass@silica sol@ loop-60000 surfaces were investigated under the same condition (ambient temperature and humidity were 22 °C and 64%, respectively). The test specimen was placed on the cooling stage with a temperature of –15 °C and a water droplet (60  $\mu L$ ) was dropped on the specimen surfaces. The whole freezing process of the water droplet was recorded by a camera (Movie S2, Supporting Information). As shown in **Figure 3**a,b, the water droplet changed from transparent to semitransparent with





www.advmatinterfaces.de

the formation of an ice shell, and the droplets became opaque with a sharp peak at the top of the droplets at the end of the freezing process. It took 170 s on the glass surface when the water droplet was completely frozen. Yet the frozen process was remarkably delayed on glass@silica sol@loop-60000 surface and the freezing time was prolonged to 1207 s, which was 7 times longer than that on the glass surface. The remarkable icing-delaying property on glass@silica sol@loop-60000 surface was attributed to the increase of the free-energy barrier for ice heterogeneous nucleation and the decrease of heat conduction. [26] Based on classic nucleation theory model, the nucleation free-energy barrier on a hydrophilic surface is relatively lower than that on a hydrophobic one, yielding a comparably lower heterogeneous nucleation rate and probability on a hydrophobic surface at a given temperature. [26a] On the other hand, the high CA results in the reduction of the interfacial contact area which could reduce the heat conduction. [26c]

In addition to icing-delaying, frosting-delay performance on glass@silica sol@loop-60000 surface also was evaluated. In a constant environment (ambient temperature 20 °C and air humidity 29%), the glass and glass@silica sol@loop-60000 surfaces were cooled to -15 °C, and the surfaces' state was recorded with a camera. As shown in Figure 3c, in the first ten seconds, it was hard to see the difference between the two surfaces because extremely tiny water droplets congealed on the surfaces. Due to the hydrophilicity and high roughness of the glass surface, it could be observed at 52 s that the glass surface has been covered with a thin layer of frost (the shadow of the camera has become blurred). But the shadow of the camera could be seen on the surface of glass@silica sol@loop-60000. which indicated that the glass@silica sol@loop-60000 surface had a low degree of frost formation. At 118 s, the glass surface turned white due to the thick frost layer on the glass surface. At 243 s, the degree of frosting on the two surfaces was very different, a clear and uniform layer of frost has formed on the glass, but the frost was just formed at the edge of glass@silica sol@loop-60000 surface and slowly spread to the surface center ( $\approx$ 243–636 s), and past 1000 s, the frost slowly covered the whole glass@silica sol@loop-60000 surface. The frosting time of the glass surface modified by the organic-inorganic hybrid coating was greatly delayed, which can be attributed to the hydrophobicity and low roughness of the surface. Finally, the two surfaces were heated up to room temperature, the hydrophilic glass surface was covered with a continuous water film, while the hydrophobic glass@silica sol@loop-60000 surface was covered with discrete droplets. The Movie S3 (Supporting Information) presented the whole process of frost formation. The frost formation in microscopic view can give a clearer perspective to detect the difference. As shown in Figure 3d,e and Movie S4 (Supporting Information), firstly, the vapor condensed on a substrate to form nanoscale droplets (Figure 3d,e) and the initial condensing time of vapor on the surface of the glass was approximately the same as that of glass@silica sol@loop-60000, ≈11 s. Due to the presence of nano-defects and hydrophilicity on the glass surface, the water droplets condensed on the glass surface were clearly different from that on glass@silica sol@ loop-60000 surface. The condensed droplets grew rapidly and froze at 86 s on glass surface. Yet on the glass@silica sol@loop-60000 surface, the size of the initially condensed micro-droplets

was more uniform and smaller, the formed droplets coalesced continuously to reduce the interface energy subsequently. At 682 s, the ice heterogeneous nucleation could be seen at the lower left inside of the vision field and began to spread to the entire surface by the ice bridge (Figure 3e). Figure 3f,g presents the condensation and frosting process on glass and glass@ silica sol@loop-60000 surfaces, which could be roughly divided into four stages: supercooled condensation, growth and coalescence, ice heterogeneous nucleation and diffusion, and frost densification. However, due to the discrepancy in wettability,<sup>[27]</sup> the filmwise condensation mode occurred on the glass surface, while dropwise condensation took place on the glass@ silica sol@loop-60000 surface. Moreover, the ice heterogeneous nucleation on the glass surface occurred all at once, while the ice heterogeneous nucleation on the glass@silica sol@loop-60000 surface preferentially occurred at the geometric boundaries and diffused through the ice bridge, which was a specific phenomenon to the hydrophobic surface of the dropwise condensation mode. [28] Besides, reducing surface energy and surface roughness are the effective means to inhibit ice heterogeneous nucleation. [29] Generally, frost occurs preferentially at a large number of physical and/or chemical defects on the solid surface, which provides effective nucleation sites for ice heterogeneous nucleation.<sup>[29a]</sup> On glass surface, there were a large number of nano-defects and protrusions that were conducive to the occurrence of ice heterogeneous nucleation. Yet, the surface of glass@silica sol@loop-60000 was smooth and with small roughness, so the probability of ice nucleation could be greatly reduced.

#### 2.4. Ice Adhesion on the Hybrid Coating Surface

It is unavoidable that the formation of ice on surfaces under extremely cold weather for a sufficient time, even if the material showed excellent icing-delay performance. When the surface is covered with ice, the most critical problem is how to remove the ice easily, and the ice adhesion strength is an important parameter to quantify the icephobic performance. Figure 4a shows the ice adhesion strength on different surfaces that are modified with various molecular weight PDMS molecules. The ice adhesion strength on glass surface reached 1.8 MPa, but after covering the hybrid coating, the ice adhesion strength reduced, and with the increase in molecular weight PDMS molecules, the ice adhesion strength reduced from ≈430 kPa to ≈150 kPa. The variation trend of ice adhesion strength on these loop-like PDMS surfaces is consistent with the change of the friction coefficient (Figure 4b). The surface modified with high molecular weight PDMS had a low friction coefficient ≈0.10, which was attributed to the hydrophobicity and flexibility of PDMS. As is illustrated in Figure 4c, the terminal groups of the high molecular weight PDMS with long molecule chain were grafted on silica sol layer, and the other parts of the PDMS molecules moved more freely, which provided better self-lubricative characteristics and lower ice adhesion. In addition, the deicing durability of the hybrid coating was also considered by a repeated icing-deicing test. As shown in Figure 4d, the glass@ silica sol@loop-60000 surface displayed excellent deicing stability and the ice adhesion strength on the glass@silica

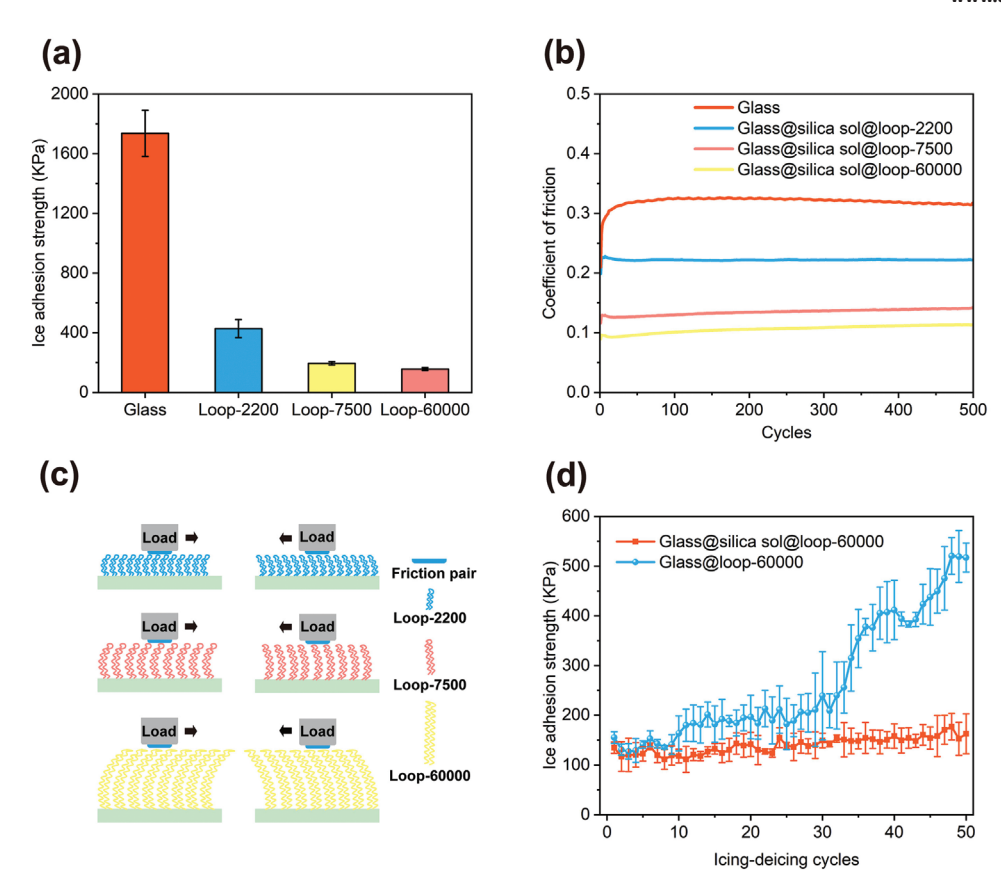


Figure 4. a) Ice adhesion strength of glass and different glass@silica sol@loop-like PDMS. b)The friction coefficient curve of glass and different glass@silica sol@loop-like PDMS. c) Schematic illustration of different glass@silica sol@loop-like PDMS during reciprocating friction test. d) Ice adhesion strength of the glass @loop-60000 and glass@silica sol@loop-60000 repeated during icing/deicing cycle tests.

sol@loop-60000 surface maintained at ≈150 kPa after 50 icingdeicing cycles. Also, the average ice adhesion strength of the 50 cycles was 139 kPa, which means the glass@silica sol@loop-60000 surface had excellent robustness. In contrast, ice adhesion on the glass@loop-60000 surface gradually increased in the repeated icing-deicing cycles, especially after 30 cycles. The ice adhesion strength had reached 519 kPa after 50 cycles. The results of repeated icing-deicing test confirmed the necessity of silica sol layer in the coating matrix. The inorganic silica sol layer not only provides ample of Si-OH group to graft a more amount of polydimethylsiloxane chains in the coating matrix, but also improves the compatibility of glass surface and makes the surface smoother (Figure 1a). More importantly, the tough silica sol layer enhances the mechanical strength of hybrid coating that guarantee low ice adhesion in repeated icingdeicing test.

#### 2.5. Self-Lubricative Performance of the Hybrid Coating Surface

To confirm the self-lubricative characteristic of glass@silica sol@loop-60000 coating, the deicing force curves on bare glass, glass@silica sol@n-octadecyltriethoxysilane surface, glass@silica sol@1H,1H,2H,2H-perfluorodecyltriethoxysilane surface and glass@silica sol@loop-60000 surface were compared at -15 °C. The deicing force curves of different specimens were

described in Figure 5a, and ice adhesion strength of different surfaces was calculated and shown in Table S2 (Supporting Information). As shown in Figure 5a, the shear force of ice on glass surface reached to 254 N, and reduced to 94 N and 53 N on glass@silica sol@n-octadecyltriethoxysilane surface and glass@silica sol@1H,1H,2H,2H-perfluorodecyltriethoxysilane surface, respectively. A similar deicing behavior was presented on the three surfaces, namely the ice block fractured away from these surfaces when the shear force increased to some extent (Movie S5, Supporting Information). On shear force curve, a sharp increase and vanish of shear force were responded. However, there was an obvious different deicing behavior on glass@ silica sol@loop-60000 surface, the ice block slid on the glass@ silica sol@loop-60000 surface with lower shear force rather than detached, which resulted in the existence of shear force even a long movement. The different deicing behavior on these surfaces could attribute to the different molecule skeletons. As displayed in Figure 5b, the n-octadecyl and 1H,1H,2H,2H-perfluorodecyl groups are C—C—C (bond angle = 109°) skeletons with poor mobility, which is considered as conventional rigid layer when grafted on the surface. [30] But for glass@silica sol@ loop-60000 surface, the Si-O-Si bond of PDMS has a large bond angle (≈143°) and dynamic flexibility, [30a] which endowed the surface with "liquid-like" self-lubricative effect. So the ice block slid rather than detached on the glass@silica sol@loop-60000 surface when applied force on it.

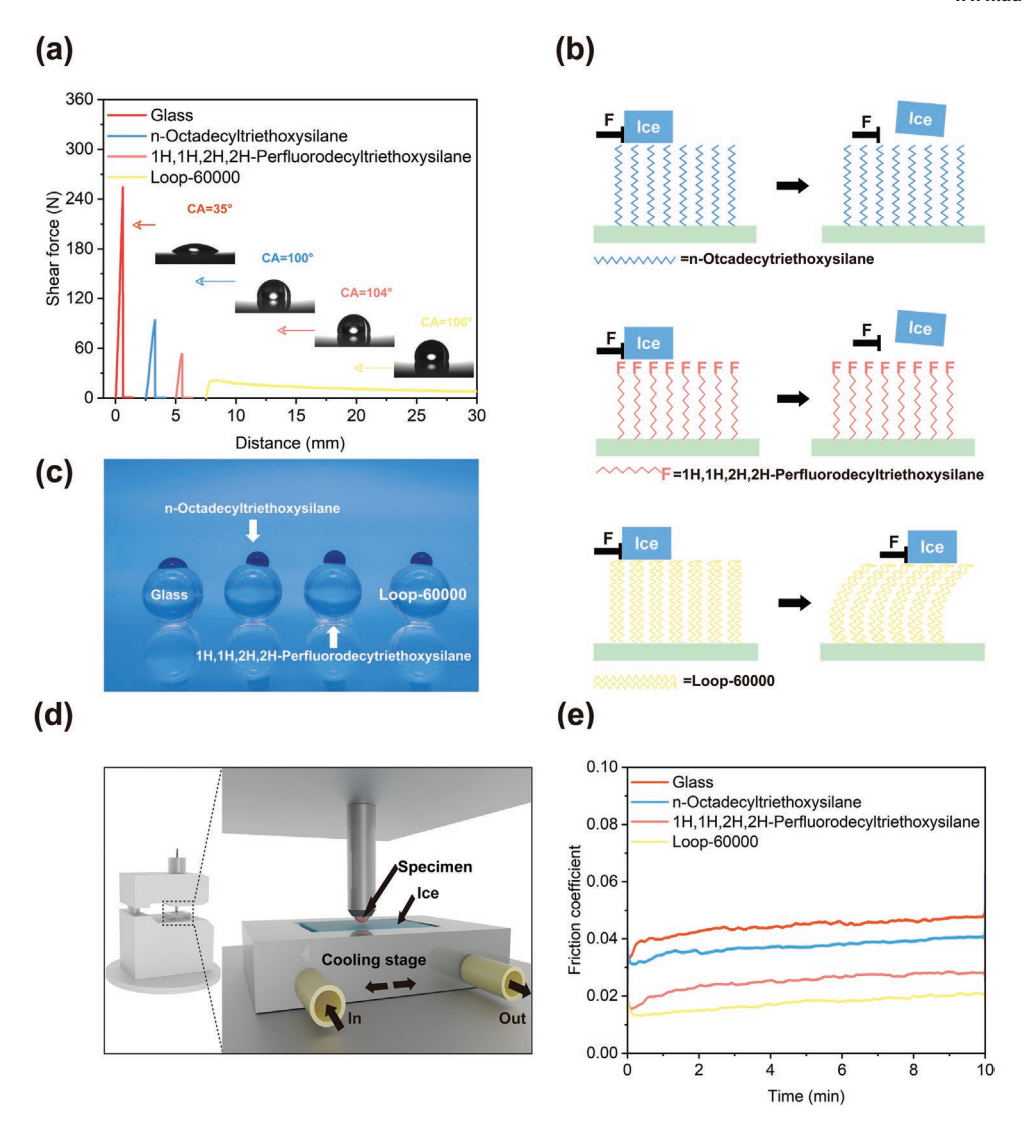


Figure 5. a) The shear force curve of ice block on glass, glass@silica sol@n-octadecyltriethoxysilane, glass@silica sol@1H,1H,2H,2H-perfluorodecyltriethoxysilane and glass@silica sol@loop-60000 surfaces. b) Schematic illustration of deicing process on glass, glass@silica sol@n-octadecyltriethoxysilane, glass@silica sol@1H,1H,2H,2H-perfluorodecyltriethoxysilane, and glass@silica sol@loop-60000 surfaces. c) Optical photographs of glass balls that coated with glass@silica sol@n-octadecyltriethoxysilane, glass@silica sol@1H,1H,2H,2H-perfluorodecyltriethoxysilane, glass@silica sol@loop-60000 coatings, respectively. d) Illustration of device for friction coefficient testing on ice. e) The friction coefficient curve of glass, glass@silica sol@n-octadecyltriethoxysilane, glass@silica sol@loop-60000 on ice surface.

To further prove the self-lubricative property of glass@ silica sol@loop-60000 surface, the friction coefficient of glass, sol@n-octadecyltriethoxysilane, glass@silica glass@silica sol@1H,1H,2H,2H-perfluorodecyltriethoxysilane and glass@ silica sol@loop-60000 coatings on the ice surface was tested. As shown in Figure 5c, the glass ball became hydrophobic after modifying the above coatings. The friction coefficient of different specimens was measured by a reciprocating tribo-tester (MFT-4000, Huahui, Figure 5d), and the friction coefficient curve and average friction coefficient are shown in Figure 5e and Table S3 (Supporting Information). The bare glass ball has the largest friction coefficient (≈0.044) on ice surface, and the friction coefficient of glass@silica sol@n-octadecyltriethoxysilane, glass@silica sol@1H,1H,2H,2H-perfluorodecyltriethoxysilane on ice surface were reduced to ≈0.037, and ≈0.025,

respectively, because of their hydrophobicity. The smallest friction coefficient (≈0.017) was presented when the glass@silica sol@loop-60000 surface rubbed on ice surface, which can attribute to the liquid-like slippery property of PDMS on the hybrid coating surface.

#### 2.6. Anti-Waxing Performance of the Hybrid Coating Surface

Paraffin is a complex mixture of *n*-alkanes, iso-alkanes and cycloalkanes, etc., and it is easy to deposit on pipeline surface to arouse flow resistance increase or even pipe blockage.<sup>[31]</sup> Because of its excellent anti-paraffin effect, low surface energy coating is the most potential application coating in pipe inner wall to reduce paraffin adhesion. Here, the anti-waxing

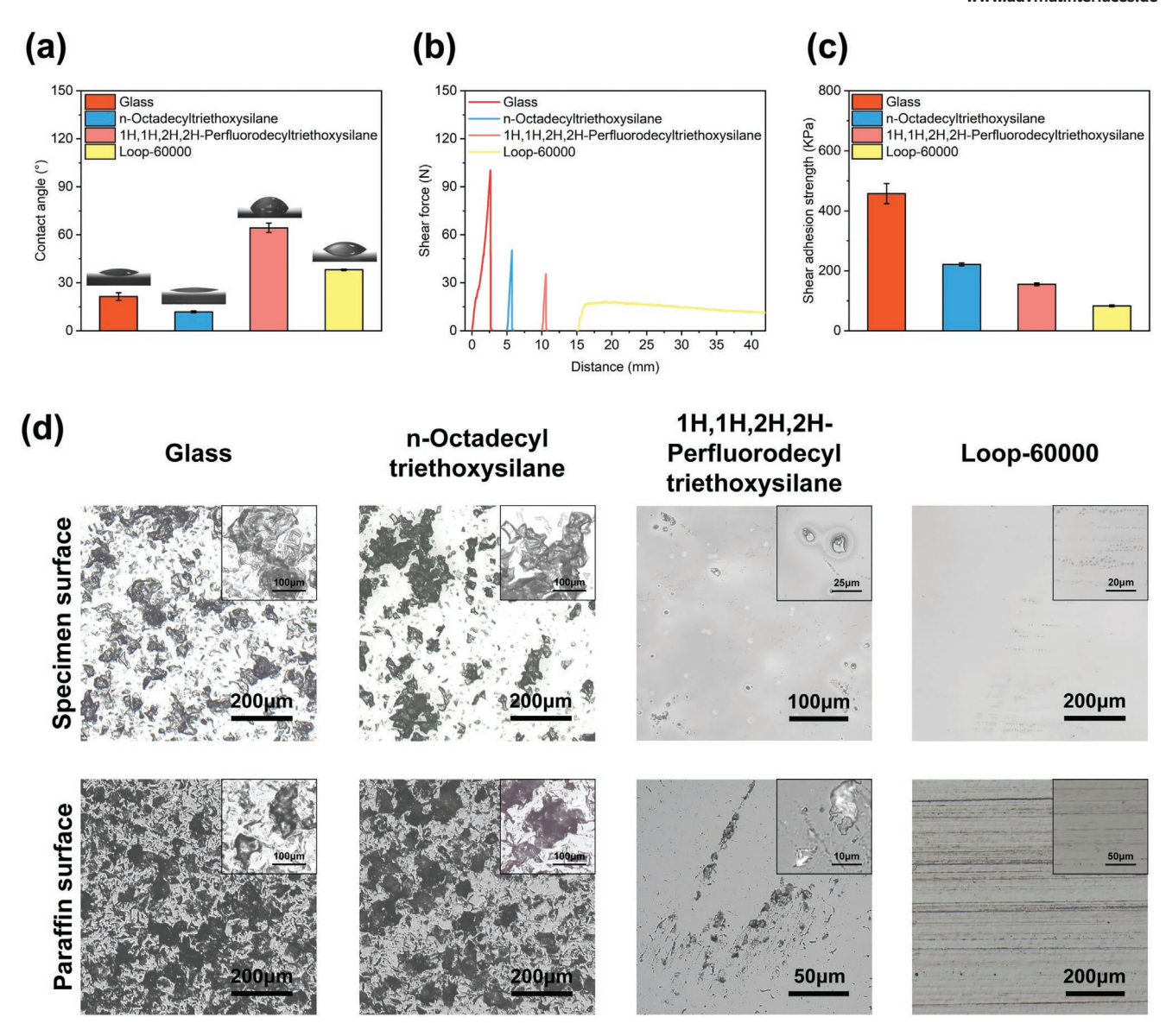


**Figure 6.** a) The paraffin CA of glass, glass@silica sol@n-octadecyltriethoxysilane, glass@silica sol@1H,1H,2H,2H-perfluorodecyltriethoxysilane and glass@silica sol@loop-60000. b) Paraffin shear force curve and c) paraffin adhesion strength of glass, glass@silica sol@n-octadecyltriethoxysilane, glass@silica sol@1H,1H,2H,2H-perfluorodecyltriethoxysilane and glass@silica sol@loop-60000. d) The microphotograph of the specimen surfaces and paraffin block after dewaxing test.

performance of loop-like PDMS surface was considered. Similar to deicing test, the specimens of glass, glass@silica sol@n-octadecyltriethoxysilane, glass@silica sol@1H,1H,2H,2H-perfluorodecyltriethoxysilane, and glass@silica sol@loop-60000 surfaces were evaluated to confirm their validity. The paraffin CA on four surfaces is summarized in **Figure 6a**. The largest paraffin CA  $\approx$ 64° was shown on glass@silica sol@1H,1H,2H,2H-perfluorodecyltriethoxysilane surface due to its oleophobicity, and because of similar compatibility, paraffin droplet spread on the surface of glass@silica sol@n-octadecyltriethoxysilane with the lowest CA  $\approx$ 12°. The paraffin CA on glass@silica sol@loop-60000 surface was  $\approx$ 38°. The paraffin adhesion force curves were shown in Figure 6b, and the paraffin adhesion strength on above surfaces was displayed in Figure 6c. Similar to ice adhesion, paraffin blocks fractured away from

glass, glass@silica sol@n-octadecyltriethoxysilane, glass@silica sol@1H,1H,2H,2H-perfluorodecyltriethoxysilane surfaces with a sharp increase of shear force, and slid on the glass@silica sol@loop-60000 surface with lower shear force rather than detached (Figure 6b), and glass@silica sol@loop-60000 had the lowest paraffin adhesion (≈83 kPa, Figure 6c.) The demonstration experiment (Movie S6, Supporting Information) visualized the difference of de-paraffin process, a paraffin block with 1 cm (length) × 1 cm (width) × 5 cm (height) was adhered to these surfaces and removed manually. The paraffin could slide on the glass@silica sol@loop-60000 surface, while it was peeled off on the surface of other specimens permanently. In addition, the micromorphology of adhesion zone was observed by a microscope to reveal the adhesion strength of paraffin on these surfaces. As shown in Figure 6d, there were lots of paraffin debris

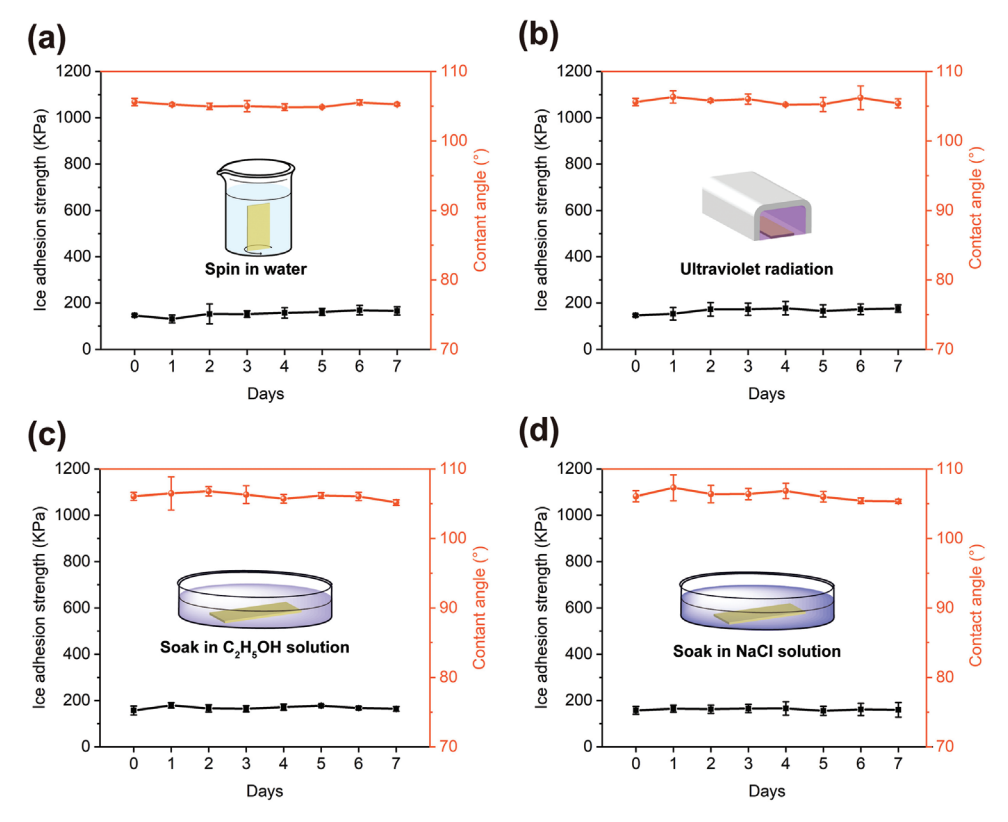


Figure 7. The durability test of glass@silica sol@loop-60000 under a) water washing, b) UV radiation, c) ethanol immersion and d) sodium chloride immersion.

on glass and glass@silica sol@n-octadecyltriethoxysilane surfaces, which means lots of paraffin matrices fractured rather than peeled off in micro scales and led to strong adhesion. For the oleophobic glass@silica sol@1H,1H,2H,2H-perfluorodecyltriethoxysilane surface, paraffin debris decreased significantly in the adhesion zone and the lower adhesion strength was presented. On glass@silica sol@loop-60000 surface, there was hardly any debris on the surface after de-waxing, and some scratches remained on the paraffin surface in the direction of push, which results in the lowest adhesion strength.

#### 2.7. Durability of the Hybrid Coating Surface

The coating durability is the most important performance that determines its potential large-scale applications in many fields. So the durability of glass@silica sol@loop-60000 coating also was considered at last. The changes in water CA and ice adhesion strength under different environments were used to evaluate its stability and durability. As shown in Figure 7, several endurance tests were conducted, including washing in water, UV irradiation, soaking in organic and saline solution. Taking the washing in water test as an example, the glass@silica sol@ loop-60000 was rotated in water at 200 rpm s<sup>-1</sup> for 7 days, and water CA and ice adhesion on the surface were detected every day during the test procedure and summarized in Figure 7a. The ice adhesion strength was maintained at ≈165 kPa and the water CA was kept at ≈105° on the surface, which means the

coating surface could endure rain washing. Similar to above test method, the changes of water CA and ice adhesion on glass@silica sol@loop-60000 surface under UV irradiation, soaking in organic and saline solution for various days were also shown in Figure 7b–d. The unchanged results confirmed the excellent stability and durability of glass@silica sol@Loop-60000 coating surface. Its stability and durability were attributed to the inert PDMS grafted on inorganic silica sol layer by covalent bond. The coating can endure various complex surroundings that also provide the possibility of application in equipment protection.

#### 3. Conclusion

In this work, a series of organic-inorganic hybrid self-lubricative coatings were successfully fabricated via a simple two-step dipping method. The long molecules chain of PDMS was grafted on solid surface with covalent bond that endowed the coating surface with good hydrophobicity, anti-stain, anti-affix, anti-ice, and anti-paraffin properties, simultaneously. Because of the flexibility and the low surface energy of PDMS, the liquid-like and self-lubricative nature of coating also was presented by comparing the ice and paraffin adhesion force on the rigid alkyl chain coating (*n*-octadecyl and 1H,1H,2H,2H-perfluorodecyl groups). The ice or paraffin block always slipped on the surface of glass@silica sol@Loop-60000 with low adhesion force, but fractured and detached from alkylated and perfluorinated coating surfaces with high adhesion strength. The coatings'





www.advmatinterfaces.de

friction behaviors on ice also confirmed their self-lubricative property. In addition, because of the covalent modification of PDMS on inorganic silica sol layer, the coating surface showed excellent stability and durability that could maintain low ice adhesion after 50 icing-deicing cycles and longtime rigorous environmental tests. This work provides evidence of the liquid-like self-lubricative property of PDMSs surface which will be helpful to design the high-performance icephobic and wax-phobic coating materials.

# 4. Experimental Section

*Materials*: Tetraethyl orthosilicate, anhydrous ethanol, and nitric acid (≈65–68%) were purchased from Sinopharm Group. Dibutyltin dilaurate (DBTDL, 95%) and 3-isocyanatopropyltriethoxysilane (95%) were purchased from Aladdin. *n*-Octadecyltriethoxysilane (95%) and 1H,1H,2H,2H-perfluorodecyltriethoxysilane (96%) were purchased from Macklin. Hydroxypropyl polydimethylsiloxane (HO-PDMS-OH, Mn = 2200, 7500, 60 000) was purchased from WSS New Material Co., LTD. Paraffin (melting point ≈50–52 °C) was purchased from Shanghai Hualing Rehabilitation Equipment Factory. Glass slides (25.4 mm × 76.2 mm) used as the substrates were obtained from Sailboat Lab Co., Ltd. The glass slides were ultrasonically cleaned with acetone, ethanol, and deionized water for 10 min sequentially, and then dried with N<sub>2</sub> and treated with O<sub>2</sub> plasma for 10 min before further use.

Preparation of Silica Sol Solution: 20 mL tetraethyl orthosilicate was added into 100 mL anhydrous ethanol and mixed thoroughly, and then 2 mL nitric acid was added into the above mixed solution under sufficient stirring. After reacting for 0.5 h, a mixed solution with 8 mL deionized water and 40 mL anhydrous ethanol was added and the reaction was continued for 1 h. Finally, the silica sol solution was aged for 24 h before usage.

Preparation of Loop-Like PDMS: The dewatered PDMS (20 g) was added into a round-bottomed flask, and 0.182 g 3-isocyanatopropyltriethoxysilane (95%) was mixed into the flask subsequently, and then 20  $\mu L$  dibutyltin dilaurate was added into the above solution and stirred 24 h at room temperature under  $N_2$  protection for reaction completely. The FTIR spectroscopy of loop-like PDMS was shown in Figure S3 (Supporting Information). To investigate the effect of PDMS molecular weight, three kinds of hydroxypropyl silicone oil, PDMS-2200, PDMS-7500 and PDMS-60000 were used to prepare the loop-like PDMS, and the products were named as loop-2200, loop-7500 and loop-60000, respectively. The reaction products could be used without further treatment, and anhydrous toluene was utilized to dilute the reaction product to 1 wt.% before usage.

Preparation of the Organic–Inorganic Hybrid Coating: Firstly, a clean glass slide was immersed in the silica sol and stood for 30 s, then the glass slide was pulled out and dried at room temperature for a few minutes. Secondly, the glass slide decorated with silica sol layer was dipped into different loop-like PDMS (loop-2200, loop-7500, and loop-60000) toluene solutions for 24 h. At last, the prepared coating was solidified by thermal treatment under 120 °C for 30 min and then washed with plenty of toluene. The obtained specimens were defined as glass@silica sol@loop-2200, glass@silica sol@loop-7500, and glass@silica sol@loop-60000, respectively. To confirm the necessity of silica sol layer, controlled specimens were also prepared, which are the glass surfaces coated with loop-like PDMS directly, and the obtained samples were named as glass@loop-2200, glass@loop-7500, and glass@loop-60000, respectively.

Characterization: The infrared spectroscopic measurement of polydimethylsiloxane was carried out on a Fourier transform infrared spectrometer (Bruker TENSOR27, KBr disks). The surface morphology of the specimens was imaged on an atomic force microscope (Bruker MultiMode®8) and the scanning electron microscopy images were observed on a field emission scanning electron microscope (FE-SEM,

JEOL JSM-6701F) at 5–10 kV. The CAs and SAs were measured with DECCA-100 optical contact-angle meter (DECCA precision instrument Co., Ltd., Shenzhen) at ambient temperature, and the droplet volume was 20  $\mu L$  and the CAs value was automatically obtained by Laplace–Young fitting algorithm. The optical micrographs were taken by a ZEISS Axiolab 5 microscope. The friction test was carried out in the reciprocating mode on friction and wear tester (MFT-R4000, Lanzhou-Huahui Instrument Technology Co., Ltd.). For friction test in air, a polyester fabric plane (5 mm  $\times$  5 mm) acted as the upper friction pair and the specimen was used as the lower friction pair. An applied load of 2 N and a frequency of 2 Hz were used as the test condition. For friction test on ice, the modified glass ball was acted as the upper friction pair, and the ice surface with a temperature of –15 °C was used as the lower friction pair, and an applied load of 8 N and frequency of 2 Hz were chosen to detect friction coefficient.

Anti-Icing and Anti-Frosting Tests: The anti-icing and macroscopical anti-frosting tests on glass and glass@silica sol@loop-60000 surfaces were performed on a cooling stage at -15 °C and the entire freezing and frosting processes were recorded with a camera. The water droplet with 60  $\mu$ L volume was used in the anti-icing test, and the ambient temperature and humidity were 22 °C and 64%, respectively. The macroscopical anti-frosting test was carried out under the conditions of ambient temperature 20 °C and air humidity 29%. The whole frosting process was observed and recorded with a ZEISS Axiolab 5 microscope.

De-Icing and De-Waxing of the Organic-Inorganic Hybrid Coating: The de-icing test was performed on an ice adhesion setup (Figure S4, Supporting Information). The test specimens were fastened onto the cooling stage, and a hollow cylindrical mold with an inner diameter of 6.75 mm and a height of 15 mm was placed on the specimen surface and injected with 1 mL of deionized water. The temperature of the cooling stage was kept at -15 °C for 2 h to ensure the ice was completely frozen, and the temperature of the cooling stage was kept at -15 °C during the entire de-icing test. The test details for the icing-deicing cycle test were the same as for the de-icing test. The de-waxing test was also carried out with the ice adhesion setup (the cooling stage was not connected to the refrigeration device), the difference was that the test specimens were fastened onto the stage with 3M tape and the molten paraffin was poured into a 1.5 cm (length)  $\times$  1.5 cm (width)  $\times$  2 cm (height) plastic mold and filled it up, and allowed it to cool naturally for 3 h. During the de-icing and de-waxing test, the force probe was moved to a position that was perpendicular to the bottom of the ice/paraffin block and close to the surface of the specimen, and to push it to move or peel off at a speed of 0.5 mm  $\ensuremath{\text{s}^{-1}}\xspace$  , and the shear force curve was transmitted by the force sensor to the adhesion force test system. In the de-icing and de-waxing tests, the adhesion strength was the average of three different samples to ensure reproducibility. In particular, three samples were used throughout the icing-deicing cycle test and the cylindrical mold was placed in the same position during each icing-deicing cycle.

Durability Test of the Organic-Inorganic Hybrid Coating: The durability of the organic-inorganic hybrid coatings was evaluated by the changes in water CA and ice adhesion strength under water washing, UV irradiation, organic solvent and salt solution soaking within 7 days. The water CA and ice adhesion strength of the glass@silica sol@loop-60000 surface were detected every day during the durability test period. In the water washing experiment, the organic-inorganic hybrid coating was rotated in water at 200 rpm s<sup>-1</sup> for 7 days. In the UV irradiation test, the organic-inorganic hybrid coating was placed under a UV light with an irradiation intensity of 3 mW cm<sup>-2</sup> for 7 days. In the organic solvent and salt solution immersion experiments, the organic-inorganic hybrid coatings were placed in ethanol solution and 1 mol L<sup>-1</sup> sodium chloride solution for 7 days, respectively.

## **Supporting Information**

Supporting Information is available from the Wiley Online Library or from the author.





www.advmatinterfaces.de

## Acknowledgements

The authors gratefully acknowledge the support by the Key Research Program of the Chinese Academy of Sciences (Grant NO. XDPB24), the National Natural Science Foundation of China (Grant NO. 22032006, 22072169), the NSAF (Grant No. U2030201), the LICP Cooperation Foundation for Young Scholars (HZJJ22-07), Young Talents Support Plan of Gansu Association for Science and Technology (GXH2020626-14).

#### **Conflict of Interest**

The authors declare no conflict of interest.

### **Data Availability Statement**

The data that support the findings of this study are available in the supplementary material of this article.

# **Keywords**

anti-icing surfaces, anti-waxing surfaces, organic-inorganic hybrid, polydimethylsiloxane, self-lubricative coating

Received: January 21, 2022 Revised: March 22, 2022 Published online:

- a) J. Chi, X. Zhang, Y. Wang, C. Shao, L. Shang, Y. Zhao, Mater. Horiz. 2021, 8, 124; b) S. Wang, K. Liu, X. Yao, L. Jiang, Chem. Rev. 2015, 115, 8230; c) B. Chang, B. Zhang, T. Sun, Small 2017, 13, 1503472; d) Y. Liu, Y. Wu, S. Liu, F. Zhou, ACS Mater. Lett. 2022, 4, 246.
- [2] a) W. Barthlott, C. Neinhuis, *Planta* 1997, 202, 1; b) H. J. Ensikat, P. Ditsche-Kuru, C. Neinhuis, W. Barthlott, *Beilstein J. Nanotechnol.* 2011, 2, 152.
- [3] a) X. Wu, Z. Chen, J. Mater. Chem. A 2018, 6, 16043; b) D. Wang,
   Q. Sun, M. J. Hokkanen, C. Zhang, F. Y. Lin, Q. Liu, S. P. Zhu,
   T. Zhou, Q. Chang, B. He, Q. Zhou, L. Chen, Z. Wang, R. H. A. Ras,
   X. Deng, Nature 2020, 582, 55; c) J. Liu, L. Ye, Y. Sun, M. Hu,
   F. Chen, S. Wegner, V. Mailander, W. Steffen, M. Kappl, H. J. Butt,
   Adv. Mater. 2020, 32, 1908008.
- [4] a) F. Sahin, N. Celik, A. Ceylan, S. Pekdemir, M. Ruzi, M. S. Onses, Chem. Eng. J. 2021, 431, 133445; b) X. Liu, X. Zhang, Q. Chen, Y. Pan, C. Liu, C. Shen, Chem. Eng. J. 2021, 406, 126532.
- [5] L. Wang, Q. Gong, S. Zhan, L. Jiang, Y. Zheng, Adv. Mater. 2016, 28, 7729.
- [6] a) D. Wei, J. Wang, S. Li, Y. Liu, D. Wang, H. Wang, Chem. Eng. J. 2021, 425, 130450; b) D. Zang, R. Zhu, W. Zhang, X. Yu, L. Lin, X. Guo, M. Liu, L. Jiang, Adv. Funct. Mater. 2017, 27, 1605446.
- [7] a) W. Wu, X. Wang, D. Wang, M. Chen, F. Zhou, W. Liu, Q. Xue, Chem. Commun. 2009, 45, 1043; b) J. Peng, S. Yuan, H. Geng, X. Zhang, M. Zhang, F. Xu, D. Lin, Y. Gao, H. Wang, Chem. Eng. J. 2022, 428, 131162.
- [8] a) G. McHale, M. I. Newton, N. J. Shirtcliffe, Soft Matter 2010, 6, 714; b) J. P. Rothstein, Annu. Rev. Fluid Mech. 2010, 42, 89; c) Y. Wu, Y. Xue, X. Pei, M. Cai, H. Duan, W. T. S. Huck, F. Zhou, Q. Xue, J. Phys. Chem. C 2014, 118, 2564.
- [9] a) T. Dong, Q. Li, N. Tian, H. Zhao, Y. Zhang, G. Han, J. Hazard. Mater. 2021, 417, 126133; b) N. Tian, S. Wu, G. Han, Y. Zhang, Q. Li,

- T. Dong, J. Hazard. Mater. 2022, 424, 127393. c) B. Wang, W. Liang, Z. Guo, W. Liu, Chem. Soc. Rev. 2015, 44, 336.
- [10] M. Ge, C. Cao, F. Liang, R. Liu, Y. Zhang, W. Zhang, T. Zhu, B. Yi, Y. Tang, Y. Lai, *Nanoscale Horiz.* 2020, 5, 65.
- [11] S. Goharshenas Moghadam, H. Parsimehr, A. Ehsani, Adv. Colloid Interface Sci. 2021, 290, 102397.
- [12] a) X. Tian, T. Verho, H. A. Ras Robin, Science 2016, 352, 142;
   b) W. Zhang, D. Wang, Z. Sun, J. Song, X. Deng, Chem. Soc. Rev. 2021, 50, 4031.
- [13] a) P. Papadopoulos, L. Mammen, X. Deng, D. Vollmer, H.-J. Butt, Proc. Natl. Acad. Sci. USA 2013, 110, 3254; b) J. Lv, Y. Song, L. Jiang, J. Wang, ACS Nano 2014, 8, 3152.
- [14] T.-S. Wong, S. H. Kang, S. K. Y. Tang, E. J. Smythe, B. D. Hatton, A. Grinthal, J. Aizenberg, *Nature* 2011, 477, 443.
- [15] a) R. J. Archer, B. Becher-Nienhaus, G. J. Dunderdale,
  A. Hozumi, Adv. Funct. Mater. 2020, 30, 1907772; b) T. L. Chen,
  Y. P. Lin, C. H. Chien, Y. C. Chen, Y. J. Yang, W. L. Wang, L. F. Chien,
  H. Y. Hsueh, Adv. Funct. Mater. 2021, 31, 2104173.
- [16] a) P. Kim, T.-S. Wong, J. Alvarenga, M. J. Kreder, W. E. Adorno-Martinez, J. Aizenberg, ACS Nano 2012, 6, 6569; b) X. Yin, Y. Zhang, D. Wang, Z. Liu, Y. Liu, X. Pei, B. Yu, F. Zhou, Adv. Funct. Mater. 2015, 25, 4237.
- [17] a) A. Sandhu, O. J. Walker, A. Nistal, K. L. Choy, A. J. Clancy, Chem. Commun. 2019, 55, 3215; b) J. Gao, Y. Zhang, W. Wei, Y. Yin, M. Liu, H. Guo, C. Zheng, P. Deng, ACS Appl. Mater. Interfaces 2019, 11, 47545; c) Y. Zhuo, V. Hakonsen, Z. He, S. Xiao, J. He, Z. Zhang, ACS Appl. Mater. Interfaces 2018, 10, 11972.
- [18] S. Heydarian, R. Jafari, G. Momen, Prog. Org. Coat. 2021, 151, 106096.
- [19] a) K. Rykaczewski, S. Anand, S. B. Subramanyam, K. K. Varanasi, Langmuir 2013, 29, 5230; b) S. Peppou-Chapman, J. K. Hong, A. Waterhouse, C. Neto, Chem. Soc. Rev. 2020, 49, 3688; c) P. Baumli, M. D'Acunzi, K. I. Hegner, A. Naga, W. S. Y. Wong, H. J. Butt, D. Vollmer, Adv. Colloid Interface Sci. 2021, 287, 102329.
- [20] a) J. Liu, Y. Sun, X. Zhou, X. Li, M. Kappl, W. Steffen, H. J. Butt, Adv. Mater. 2021, 33, 2100237; b) L. Zhang, Z. Guo, J. Sarma, X. Dai, ACS Appl. Mater. Interfaces 2020, 12, 20084; c) L. Wang, T. J. McCarthy, Angew. Chem., Int. Ed. Engl. 2016, 55, 244; d) A. K. Halvey, B. Macdonald, K. Golovin, M. Boban, A. Dhyani, D. H. Lee, J. W. Gose, S. L. Ceccio, A. Tuteja, ACS Appl. Mater. Interfaces 2021, 13, 53171; e) X. Zhong, L. Lv, H. Hu, X. Jiang, H. Fu, Chem. Eng. J. 2020, 382, 123042; f) M. Rabnawaz, G. Liu, H. Hu, Angew. Chem., Int. Ed. Engl. 2015, 54, 12722; g) Y. Zhuo, S. Xiao, A. Amirfazli, J. He, Z. Zhang, Chem. Eng. J. 2021, 405, 127088; h) M. Rabnawaz, G. Liu, Angew. Chem., Int. Ed. Engl. 2015, 54, 6516; i) J. Yang, J. Li, X. Jia, Y. Li, H. Song, ACS Appl. Mater. Interfaces 2020, 12, 28645; j) Z. Ma, Y. Wu, R. Xu, Z. Li, Y. Liu, J. Liu, M. Cai, W. Bu, F. Zhou, ACS Appl. Mater. Interfaces 2021, 13, 14562.
- [21] J. V. Buddingh, A. Hozumi, G. Liu, Prog. Polym. Sci. 2021, 123, 101468.
- [22] a) B. Shang, M. Chen, L. Wu, ACS Appl. Mater. Interfaces 2018, 10, 41824; b) P. Liu, H. Zhang, W. He, H. Li, J. Jiang, M. Liu, H. Sun, M. He, J. Cui, L. Jiang, X. Yao, ACS Nano 2017, 11, 2248; c) Z. Ma, Y. Wu, R. Xu, Y. Liu, Z. Li, J. Liu, X. Pei, W. Bu, F. Zhou, Prog. Org. Coat. 2021, 154, 106171; d) Y. Liu, C. Qin, R. Xu, Y. Liu, Y. Wu, B. Yu, X. Pei, F. Zhou, Langmuir 2022, 38, 2832.
- [23] a) K. Zhang, S. Huang, J. Wang, G. Liu, Angew. Chem., Int. Ed. Engl. 2019, 58, 12004; b) L. Lei, J. Buddingh, J. Wang, G. Liu, Chem. Eng. J. 2020, 380, 122554.
- [24] J. Wang, L. Wang, N. Sun, R. Tierney, H. Li, M. Corsetti, L. Williams, P. K. Wong, T.-S. Wong, Nat. Sustain. 2019, 2, 1097.
- [25] D. K. Owens, R. C. Wendt, J. Appl. Polym. Sci. 1969, 13, 1741.
- [26] a) W. Xu, Z. Lan, B. L. Peng, R. F. Wen, X. H. Ma, J. Chem. Phys. 2015, 142, 054701; b) Z. Zhang, X. Y. Liu, Chem. Soc. Rev. 2018, 47, 7116; c) A. Alizadeh, M. Yamada, R. Li, W. Shang, S. Otta, S. Zhong,





www.advmatinterfaces.de

- L. Ge, A. Dhinojwala, K. R. Conway, V. Bahadur, A. J. Vinciquerra, B. Stephens, M. L. Blohm, *Langmuir* **2012**, *28*, 3180.
- [27] Y. Hou, M. Yu, X. Chen, Z. Wang, S. Yao, ACS Nano 2015, 9, 71
- [28] S. Nath, S. F. Ahmadi, J. B. Boreyko, Nanoscale Microscale Thermophys. Eng. 2017, 21, 81.
- [29] a) J. B. Boreyko, C. P. Collier, ACS Nano 2013, 7, 1618; b) X. X. Zhang, M. Chen, M. Fu, J. Chem. Phys. 2014, 141, 124709.
- [30] a) L. Zhang, Z. Guo, J. Sarma, W. Zhao, X. Dai, Adv. Funct. Mater. 2021, 31, 2008614; b) D. F. Cheng, B. Masheder, C. Urata, A. Hozumi, Langmuir 2013, 29, 11322.
- [31] J. Bai, X. Jin, J.-T. Wu, Pet. Sci. 2019, 16, 619.